

Daytime long-wave radiation approximation for physical hydrological modelling of snowmelt: a case study of southwestern Ontario

S. R. FASSNACHT

Department of Hydrology and Water Resources, University of Arizona, Tucson, Arizona 85721-0011, USA

e-mail: srfassna@hwr.arizona.edu

K. R. SNELGROVE & E. D. SOULIS

Department of Civil Engineering, University of Waterloo, Waterloo, Ontario N2L 3G1, Canada

Abstract Since incoming long-wave radiation is not routinely measured in Canada, when it is required as a meteorological parameter, such as input to a physically-based hydrological model, the data must be derived. These data have been successfully computed as a function of near surface air temperature and cloud cover. However, cloud cover data are also not routinely measured. A method is described to compute the cloud cover fraction, for use to estimate the long-wave radiation, from a comparison of measured to theoretical short-wave radiation at three sites in central southwestern Ontario. The daytime cloud cover fraction is on average slightly more than 0.50. The impact of different long-wave radiation estimates from varying cloud cover fraction assumptions is illustrated in terms of simulated streamflow resulting from snowmelt.

Key words incoming long-wave radiation; short-wave radiation; snowmelt modelling; cloud cover

INTRODUCTION

Physically-based hydrological modelling requires good estimates of the radiation balance. Most models use an approximation of the radiation spectrum by dividing it into the bands of short-wave or solar ($<4 \mu\text{m}$) and long-wave or terrestrial ($4\text{--}50 \mu\text{m}$) radiation. For snowmelt modelling, especially in mid-latitude non-alpine regions where melt occurs in March or April, daily total incoming long-wave radiation quantities are usually greater than short-wave radiation levels (Hütter & Schneider, 1975). During the day there is a strong correlation between incoming short-wave and long-wave radiation; as cloud cover increases, short-wave radiation decrease due to cloud top reflection, while incoming long-wave radiation is enhanced due to the increased emissivity of cloudy skies. During the night this correlation no longer exists, since there is no short-wave radiation. At meteorological stations, short-wave radiation is more readily measured than long-wave radiation. Both long- and short-wave radiation can be derived where no measurements exist; however, the requirement for a cloudiness fraction is essential to both derivations.

For modelling the snowmelt hydrology of several watersheds in southern Ontario, Canada, an assumption of a 0.50 cloud cover fraction throughout the year was used by Snelgrove (1996) to estimate long-wave radiation. The validity of this assumption was not quantified. Although no long-wave radiation measurements are available, short-wave radiation was measured at a number of locations in the study area. The goal of this paper is to assess the impact of changes to the 0.5 cloud cover assumption by incorporating a derived cloudiness index based on short-wave radiation measurements. The sensitivity of these changes will be assessed through comparison of streamflows generated by snowmelt hydrological modelling.

METHODOLOGY

Hydrological modelling

The physical model WATCLASS (WATflood + CLASS) is used to model the winter hydrology (see Soulis *et al.*, 2000 for details). This model is a linkage between the Canadian Land Surface Scheme, CLASS, developed by the Meteorological Service of Canada (Verseghy, 2000) and the WATFLOOD (WATERloo FLOOD forecasting) hydrological model developed at the University of Waterloo (Kouwen *et al.*, 1993). The water and energy balances are modelled in the vertical direction. There are three soil layers and four subareas (bare soil, canopy covered, snow covered, snow and canopy covered) for each grid cell. Water can either remain on the surface as ponded water, infiltrate into the soil and be stored, or drain off the surface as overland flow, from the upper soil layers as interflow, or from the bottom of the soil column as a contribution to base flow. Within the soil, heat is transferred by conduction and advection, and soil moisture is moved according to Richards' equation. The canopy can be represented by up to four different vegetation types: coniferous, deciduous, crops and grasses. The evolution of each soil layer is defined by the mean temperature and soil moisture content (liquid and frozen). The evolution of the canopy is defined by its temperature, moisture storage (liquid and frozen), the growth index, and albedo (both the near-infrared and visible components), while the emissivity of the surface is assumed to be unity for all calculations. The evolution of the snowpack is defined by its temperature, snow water equivalent, density, and albedo. The heat capacity and thermal conductivity are calculated as function of the snowpack density. The loss of snow through sublimation is calculated using the bulk transfer formulae.

The grouped response unit (GRU) approach to land cover types (see Kouwen *et al.*, 1993) enables distributed (or mosaic) modelling. This approach assumes that, within a grid element, land cover dictates soil properties and individual land cover patches within a grid-element can be grouped together for modelling. Runoff is generated as surface runoff, interflow and groundwater flow, and summed for each of the ground elements. Runoff reaching the stream channels is routed using a channel routing model.

The model uses the following seven meteorological forcing parameters: air temperature, precipitation, air pressure, specific humidity, wind speed, and short-wave and long-wave radiation. Station hourly meteorological data were gridded using the inverse weighted distance technique, as per Tao & Kouwen (1989).

Cloud cover estimation

Long-wave radiation is not routinely measured in Canada, while short-wave radiation is measured at approximately 90 locations (Environment Canada, 1998). However, the incoming long-wave radiation (L_{in}) can be approximately calculated from the near surface air temperature (T_a) by the Stefan-Boltzmann equation, as follows:

$$L_{in} = \epsilon_{at} \sigma T_a^4 \quad (1)$$

where ϵ_{at} is the integrated effective emissivity of the atmosphere and canopy, and σ is the Stefan-Boltzmann constant ($\sigma = 5.6697 \times 10^{-7} \text{ W m}^{-2} \text{ K}^{-4}$) (Dingman, 1994). For no forest canopy, such as meteorological stations, Croley (1989) estimated ϵ_{at} as a function of the near surface vapour pressure (e_a in kPa) and an estimate of the fraction of cloud cover (C_{cloud}), based on the work by Brunt (1932):

$$\epsilon_{at} = (0.53 + 0.2055e_a^{0.5})(1 + 0.40C_{cloud}) \quad (2)$$

It should be noted that under completely cloudy and very moist conditions, ϵ_{at} can be computed to be larger than unity, and thus equation (2) should be used with caution under such conditions in order to not overestimate the incoming long-wave radiation.

Since the fraction of cloud cover is often unknown, it can be derived as a comparison of the measured solar radiation to the theoretical value, during daylight hours. The sensitivity of the cloud fraction can be assessed from equation (2) to have a linear impact ranging from no cloud cover to an increase of 40% with total cloud cover.

For no canopy, the incoming instantaneous solar radiation flux on a horizontal plane (K_{in}) can be expressed as follows:

$$K_{in} = I_{sc} E_o (\cos \delta \cos \Lambda \cos \omega t_{\Delta SN} + \sin \delta \sin \Lambda) [0.355 + 0.68(1 - C_{cloud})] \quad (3)$$

where I_{sc} is a solar constant ($I_{sc} = 1367 \text{ W m}^{-2}$), E_o is the eccentricity correction, δ is the declination in degrees, Λ is the latitude, ω is the angular velocity of the Earth's rotation (15° h^{-1}), and $t_{\Delta SN}$ is the time (h) before (negative) or after (positive) solar noon. The cloud cover component was initially approximated by Gray *et al.* (1973) from daily average solar radiation measurements. The eccentricity correction is a measure of the distance between the Earth and the Sun. The declination is the latitude at which the sun is directly overhead (solar noon). Both E_o and δ can be approximated by Spencer (1971), and require an estimation of the day angle (ϑ), which is the position of the Earth in its orbit. The day angle is a function of the Julian day and can be computed from Iqbal (1983).

If the measurement of solar radiation occurs with respect to local time at a measurement station, it is necessary to convert the measurement time to local apparent time (LAT), which is a measure of t , i.e. it considers the local time of solar noon. This computation uses the equation of time, which is the discrepancy in the length of the solar day and the time at which solar noon occurs over the course of the year. It can be approximated from Spencer (1971).

From measured values of incoming solar radiation at a specified time of day and year and at the specified location, the fraction of cloud cover (to be used in equation (2)) can be estimated as a function of the measured incoming solar radiation

(K_{meas}) and the theoretical quantity (K_{in}) by solving equation (3) for cloud cover:

$$C_{\text{cloud}} = 1 - \frac{1}{0.68} \left[\frac{K_{\text{meas}}}{K_{\text{in}}} - 0.355 \right] \quad (4)$$

STUDY AREA

The modelling concentrates on the Upper Grand River basin in central southwestern Ontario (Fig. 1). The drainage area for the outflow of the basin is 3520 km². This area of Canada receives from 800 to 1000 mm of precipitation annually, of which one third often comes in the form of snow. In an average year, snowmelt begins in mid March in the south and by mid April in the northern part of the study area. While the winter is usually mild with minimum temperatures reaching -10 to -15°C, extended periods of -25 to -30°C have been observed.

The hydrological parameters have been well established for this basin (Kouwen *et al.*, 1993), and 10 by 10 km grid elements are used with six different land cover types. Most of this basin is covered by crops and low vegetation (59%), with smaller regions of wetland (18%) and mixed deciduous-coniferous forest (14%). The remainder of the

Table 1 Southern Ontario meteorological gauges that measure short-wave radiation.

Station: number	name	Elevation (m a.s.l.)	Latitude (N)	Longitude (W)
6142285	Elora Research Station	376	43°39'	80°25'
6158350	Toronto	113	43°40'	79°24'
611KBEO	Egbert CARE	252	44°14'	79°47'

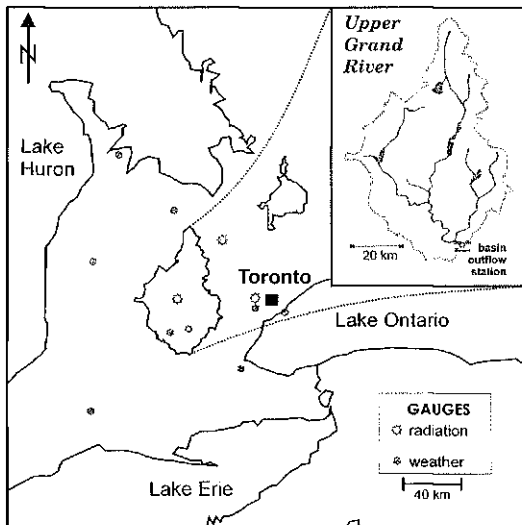


Fig. 1 Map of central southwestern Ontario illustrating the location of the Upper Grand River basin.

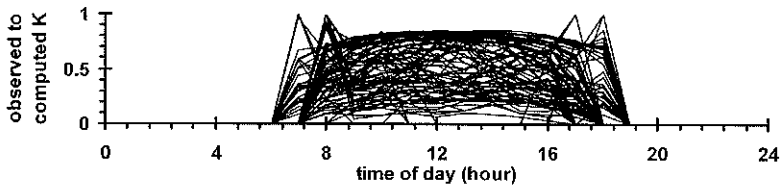


Fig. 2 Ratio of measured to computed clear-sky hourly short-wave radiation for the MSC meteorological station at Egbert CARE over the winter of 1993.

basin comprises bare (8%) and impervious (1%) areas. The terrain in this portion of southern Ontario is glacial material, composed primarily of clayey till.

Short-wave radiation data were available at three stations in southern Ontario (Table 1).

DATA INVESTIGATION

The observed short-wave radiation (K_{meas}) was compared to the computed clear-sky short-wave radiation (K_{inc}). The plot for the Egbert CARE station (Fig. 2) is typical and produces an envelope of values. The top of the envelope are the maximum ratios, corresponding to clear-sky observations. For most periods of the winter, this maximum ratio is less than unity, due in part to extinction of a small portion of the solar radiation from atmospheric particulates. The extreme morning and evening ratios (around sunrise and sunset) occur due to numerical instability (division of small numbers) and instrumentation error at very low radiation measurements. A distinct pattern is presented that is approximately symmetrical about solar noon. While the shapes of the maximum ratio curves are similar for the three stations, the largest value at solar noon ratios for both Egbert CARE and Elora are 0.84 and for Toronto is 0.79. We speculate that this 5% decrease for Toronto is influenced by absorption of solar radiation by atmospheric particulate pollution. The maximum K_{meas} to K_{inc} ratios for the Toronto station were computed separately from the other two stations. The sets of ratios were divided into different time periods to consider the variation in the length of a day. It was found that over the 5-year period, the pattern of maximum K_{meas} to K_{inc} ratios for each time period repeated annually. The maximum ratio increased as the length of day increased. A third order polynomial was fitted to each set of data with r^2 values ranging from 0.975 to 0.992.

RESULTS AND DISCUSSION

The polynomials derived from the maximum K_{meas} to K_{inc} ratios correspond to the assumption that the maximum non-unity ratio is the clear-sky value. When the computed clear-sky short-wave radiation was reduced by the maximum ratios (to consider clear-sky observations when the maximum ratio was less than unity), the average cloud coverage for all the observations was 0.54, 0.55, and 0.60, with a maximum variation of 0.11 (Table 2). When the default value of 0.5 was used for missing data and during the nights, the average cloud cover fractions reduced to 0.52,

Table 2 Average cloud cover fraction at the AES CARE, Elora and Toronto meteorological stations as derived from the difference between measured short-wave and clear-sky short-wave radiation, using all data and daytime data.

Winter	All data:			No night or missing data:		
	CARE	Elora	Toronto	CARE	Elora	Toronto
1993	0.53	0.57	0.55	0.58	0.58	0.61
1994	0.52	0.53	0.54	0.56	0.57	0.58
1995	0.53	0.53	0.54	0.56	0.57	0.59
1996	0.49	0.49	0.54	0.47	0.48	0.63
1997	0.52	0.51	0.54	0.56	0.53	0.59
all	0.52	0.52	0.54	0.54	0.55	0.6

Note: The method considers that there is typically less than 100% of the theoretical clear-sky radiation reaches the Earth's surface and that the morning and late afternoon short-wave measurement are low due.

0.52, and 0.54, for Egbert CARE, Elora, and Toronto, with maximum variations of 0.04, 0.08, and 0.01, respectively. These cloud cover fractions approach the initial assumption of 50% cloud cover on average. However, when an average value is used the daily fluctuations are not considered and this is crucial for modelling snowmelt.

The effect of a number of constant cloud cover fractions together with the effect of variable cloud cover derived from the short-wave radiation observations is illustrated in the initial spring snowmelt hydrographs in Fig. 3(a) (21 March–3 April 1993). With a 100% cloud cover simulation the total emissivity is too large resulting in too much long-wave radiation, and thus snowmelt occurs too fast. Conversely, no cloud cover (0%) results in too little long-wave radiation as there is no emissivity impact from clouds and snowmelt occurs too slowly. The melt water (using 0% cloud cover) appears later in the spring as an overestimate of streamflow, as illustrated in Fig. 3(b).

The hydrographs derived from both the 50% and variable cloud coverages are very similar. There is slightly less water initially, in the order of 10%, and more water during the recession of the first major snowmelt peak on 30 March. There is a significant impact on the hydrographs from the derived long-wave radiation. However, there are other issues for the simulated hydrographs not matching the observed values, including frozen ground parameterization and winter precipitation estimation. These are beyond the scope of this paper.

Future modelling will use atmospheric model data as the meteorological input. However, estimation of cloud cover in climate models is still difficult (Miller, personal communication, 2000). Use of station data will thus continue to supplement modelled meteorological data.

CONCLUSIONS AND RECOMMENDATIONS

While the long-wave radiation at a location can be computed from the near surface air temperature, an estimate of the cloud cover fraction is necessary. For areas such as southern Ontario the cloud cover fraction is an important consideration in hydrological modelling. The cloud cover fraction can vary from 0.0 to 1.0, resulting in a variation of the long-wave radiation of 40%. This in turn can significantly alter the surface energy balance and in particular the rate of snowmelt. For the daytime hours, a method was

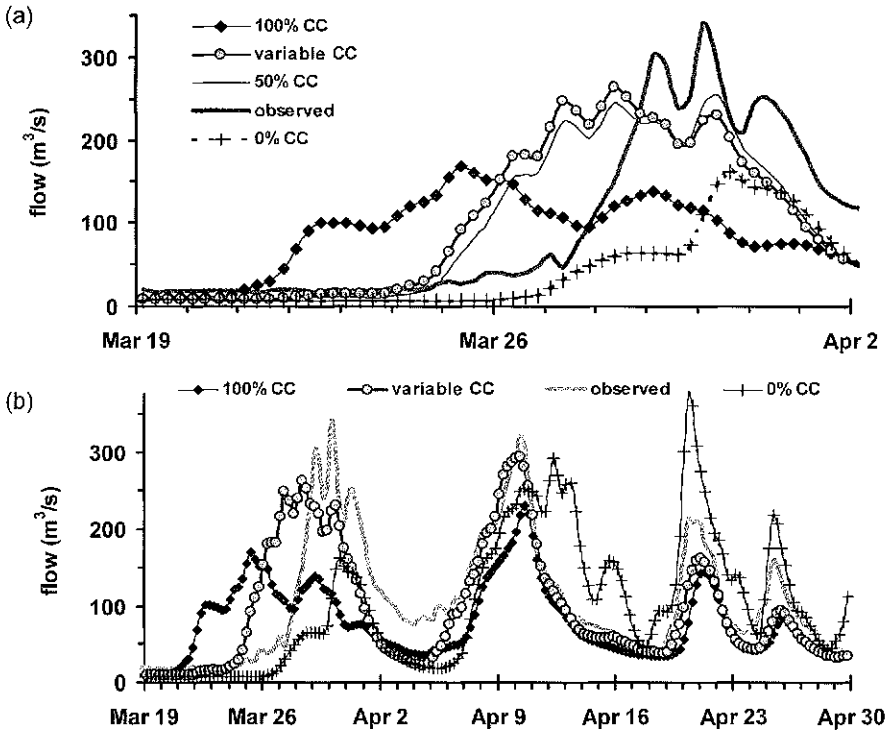


Fig. 3 Effect of cloud cover percentage used to calculate long-wave radiation fluxes on initial spring peak: (a) for the Grand River at Galt in 1993 (24 March–9 April); and (b) for the entire snowmelt period (100, variable and 0% cloud cover).

illustrated to estimate the cloud cover fraction for long-wave radiation computation using a comparison of the measured and theoretical clear-sky short-wave radiation. The average daytime cloud cover fraction for three locations in central southwestern Ontario (Egbert CARE, Elora and Toronto) for five winters ranged from 0.54 to 0.60.

Since the comparison of measured to theoretical short-wave radiation for cloud cover estimation is only useful for daylight hours, assumptions are required for non-daylight hours. The method should be tested with a complete set of radiation measurements. As atmospheric models become more robust, their output can be used directly as input to physically-based hydrological models to overcome the lack of long-wave radiation measurements. Meteorological gauge data should continue to be used for evaluation and adjustment of model output.

Acknowledgements This research was supported by Meteorological Service of Canada (MSC) Science Subventions, MSC-CRYSYS funding, and MSC-CCRNet Land-Air Node funding. Dr D. L. Verseghy of MSC, Downsview, Ontario, Canada, provided the CLASS code and Dr N. Kouwen of the University of Waterloo, Ontario, Canada, provided the WATFLOOD code and the Grand River basin parameter files. Thanks are also due to MSC-Climate Archive for the data provided. Dr N. Miller of the Lawrence Berkeley National Laboratory, Berkeley, California provided very

insightful comments on the atmospheric modelling of cloud cover. Completion of this paper was funded by the NASA Earth Observation System Southwest Regional Earth Science Applications Center (SW RESAC) located at the Department of Hydrology and Water Resources of the University of Arizona, Tucson, Arizona.

REFERENCES

- Brunt, D. (1932) Notes on radiation in the atmosphere, I. *Quart. J. Roy. Met. Soc.* **58**, 389–418.
- Croley, T. E. II (1989) Verifiable evaporation modelling on the Laurentian Great lakes. *Wat. Resour. Res.* **25**(5), 781–792.
- Dingman, S. L. (1994) *Physical Hydrology*. Prentice Hall, Englewood Cliffs, New Jersey, USA.
- Environment Canada (1998) CMC Climate And Water Information: Canadian Climate Station Catalogue. <http://www1.tor.on.ca/csc/query.asp>. Canadian Meteorological Centre, Atmospheric Environment Service, Downsview, Ontario, Canada.
- Gray, D. M., McKay, G. A. & Wigham, J. M. (1973) Energy, evaporation, and evapotranspiration. In: *Handbook on the Principles of Hydrology* (ed. by D. M. Gray). Water Information Centre, New York, USA.
- Hütter, R. & Schneider, F. (1975) Antenne. In: *Radio-Activität* no. 8, Kling Klang 1C 062 82 087, Düsseldorf, Germany.
- Iqbal, M. (1983) *An Introduction to Solar Radiation*. Academic Press, Toronto, Canada.
- Kouwen, N., Soulis, F. D., Pietroniro, A., Donald, J. & Harrington, R. A. (1993) Grouped Response Units for distributed hydrologic modeling. *J. Wat. Resour. Plan. Manage.* **119**(3), 289–305.
- Snelgrove, K. R. (1996) Hydrologic computing modelling using the WATFLOOD hydrologic model and the Canadian Land Surface Scheme (CLASS). Unpublished MAsc project, Dept of Civil Engng, Univ. of Waterloo, Ontario, Canada.
- Soulis, F. D., Snelgrove, K. R., Kouwen, N., Seglenieks, F. R. & Verseghy, D. L. (2000) Toward closing the vertical water balance in Canadian atmospheric models: coupling of the land surface scheme CLASS with the distributed hydrological model WATFLOOD. *Atmosphere–Ocean* **38**(1), 251–269.
- Spencer, J. W. (1971) Fourier series representation of the position of the Sun. *Search* **2**(5), 172.
- Tao, T. & Kouwen, N. (1989) Remote sensing and fully distributed modelling for flood forecasting. *J. Wat. Resour. Plan. Manage.* **115**(6), 809–823.
- Verseghy, D. L. (2000) The Canadian Land Surface Scheme (CLASS): its history and future. *Atmosphere–Ocean* **38**(1), 1–13.